RESEARCH PAPER

Crushing performances and crashworthiness optimization of polygonal double tubes under multiple angle loadings

Zhichao Li[1] · Haimin Zhu[1] · Chaofeng Yang[2]

Abstract

A finite element model of a thin-walled square tube is developed for evaluating its crushing performance. The axial crushing behavior of the square tube is experimentally evaluated, and the obtained force–displacement responses are applied to estimate the accuracy of the model. The validated model is subsequently used to study the crushing performances of the polygonal single and double tubes under different angle loadings. It is shown that the double tube has higher specific energy absorption and energy absorption capacity under axial and small-angle oblique loadings. However, the energy absorption characteristics of the double tube are more sensitive to the loading angle, and it is more prone to occur global bending deformation under loadings at large angles. The energy absorption characteristics of the polygonal double tubes with different cross-sectional forms are calculated and ranked. The results show that the B9 double tube has the best comprehensive performance. The B9 double tube is constructed with a gradient thickness instead of a uniform thickness to improve its crushing performance under large-angle loadings and raise its critical angle of occurring global bending deformation. A multiobjective optimization procedure is proposed to find the optimal design of the FGT double tube for enhanced crashworthiness performance.

1 Introduction

A single-tube thin-walled structure has excellent energy absorption capacity and is extensively utilized in automotive, rail transportation, aerospace, and other fields. It is possible to improve the energy absorption characteristics of a single tube via careful consideration of its cross-sectional form, geometric dimensions, material property, and other factors (Kim and Lee 1999; Yang and Qi 2013). However, the space utilization rate of the single tube is relatively poor, and a significant portion of the available space inside it is wasted, except for the area taken up by the wall thickness. In addition, when the length of its sides grows, the space

occupancy rate rises, but the space utilization rate drops. The most straightforward way to enhance the space utilization rate of a single tube is to put hollow tubes inside it, converting it from a single-tube to a multi-tube structure.

Compared to a single tube structure, a multi-tube structure may exploit the interaction between the tube walls during the crushing deformation process to enhance the energy absorption properties. Kashani et al. (2013) investigated the axial crushing behaviors of the bi-tubular square tubes using experiments and numerical modeling, as well as the influence of various inner square tube arrangements on the quasi-static axial crushing response. Changing the location of the inner tube improves the interaction between the inner and outer tubes and the energy absorption capacity of the double tubes. Sharifi et al. (2015) examined the axial crushing deformation of double circular tubes and explored the impacts of wall thickness, diameter, and the interaction between the inner and outer tubes. It may be possible to improve the interaction behaviors by decreasing the distance between the inner and outer tubes. Nia and Khodabakhsh (2015) found that the diameters of the inner and outer tubes impact the dynamic and static energy absorption properties

✉ Haimin Zhu
hamy_zhu@163.com

1   School of Automotive Engineering, Changshu Institute of Technology, Changshu 215500, Jiangsu, China

2   AnHui ZhongDing NVH Co., Ltd., NingGuo 242300, Anhui, China

of double circular tubes. Zheng et al. (2014) employed the finite element approach to explore the axial crushing behaviors of polygonal single and double tubes with foam-filled and empty and evaluate the effects of different impact velocities on their axial crushing characteristics. Vinayagar and Kumar (2017) performed quasi-static axial compression experiments on bi-tubular structures with double sections. The double-section tubes have a greater average crushing load and higher specific energy absorption than the single tubes, and their energy absorption efficiency increases by 132–213%. Rahi (2018) conducted research on the axial crushing characteristics of combined double tubes comprised of circular and square tubes and discovered that using double tubes can change the unstable deformation of a single tube during the crushing deformation process, allowing them to have better energy absorption characteristics.

In addition to double-tube structures, the energy absorption characteristics of multi-tube structures have also garnered considerable attention. Goel (2015) conducted an investigation of the axial collapse characteristics of single-, double-, and multiple-tube structures using the finite element approach. The double and multiple tubes have a higher value in terms of the energy absorption effectiveness factor than single tubes. Nia and Chahardoli (2016a, b) studied the axial crushing characteristics of three-tube structures through experiments and numerical simulation. Three-tube structures have better specific energy absorption and crushing force efficiency at the same mass, wall thickness, and height as single tubes. If the mass, wall thickness, and height of the multi-tube structures remain unchanged, increasing the number of tubes inside them will result in an increase in the specific energy absorption and crushing force efficiency. Nevertheless, this will have almost no effect on the maximum peak load. A novel three-tube configuration with circular inner and outer tubes and a star or corrugated tube in the center was proposed by Liu et al. (2016) and Deng et al. (2019). The energy-absorbing ability of the new structure is significantly improved because of the heightened interaction between its three tubes during the axial crushing deformation process. In addition, the axial energy absorption performances of the embedded multi-tube structures have been examined by Güden and Kavi (2006), Zhang et al. (2017), and Gan et al. (2018), with findings indicating that the interaction between the inner and outer tubes may enhance the structure's ability to absorb energy.

In terms of oblique loads, the axial and oblique crushing properties of hollow and foam-filled double circular tubes were investigated by Djamaluddin et al. (2015). When subjected to axial loading, the double tubes deform in a progressive collapse mode to efficiently absorb impact energy. However, the collapse deformation mode of the double tubes changes under oblique loads at 30°, and the impact energy is mainly consumed by global bending deformation, resulting in a considerable reduction in energy absorption capacity. The energy absorption characteristics of foam-filled double circular tubes and double elliptical ones were examined by Gao et al. (2016b, a) under multiple angle loadings. The findings revealed that foam-filled double elliptical tubes have better energy absorption characteristics. When subjected to oblique loading, the specific energy absorption and initial peak force of the double tubes experience a degree of reduction. This reduction is particularly pronounced following the occurrence of global bending deformation, at which point the specific energy absorption of the double tubes decreases substantially. Djamaluddin (2023) compared the axial crushing characteristics of a double tube made up of circular and polygonal tubes and found that the double tube with an octagonal inner tube has the best axial crushing performance. The oblique crushing behaviors of the circular-octagonal double tube were investigated, and its total energy absorption, specific energy absorption, and initial peak load decreased as the loading angle increased.

To sum up, the space utilization rate and energy absorption capacity of the multi-tube structures are superior to those of the single tubes under axial loads. However, there are currently only a limited number of studies on the oblique crushing properties of multi-tube structures. It is necessary to conduct research to determine whether or not the oblique crushing properties of multi-tube structures are superior to those of single tubes. This paper focuses on the crushing behaviors of polygonal double tubes under different loading angles. It also provides theoretical guidance for the rational design of double-tube structures under uncertain loads. This paper aims to gain a comprehensive understanding of multi-tube structures.

2 Geometric configuration of double tubes

The material used for the polygonal double tubes structures is aluminum alloy AL6060-T4. The mechanical properties of this material are Young's modulus 70GPa, yield stress 71 MPa, and Poisson's ratio 0.3. Figure 1 shows polygonal double-tube structures with different cross-sectional shapes. The circumscribed circle diameters of the inner and outer tubes for double tubes are 80 mm and 100 mm, respectively, as illustrated in Fig. 2, and their wall thickness and length are 2 mm and 240 mm, respectively. To make the subsequent analysis more manageable, the polygonal double tubes are referred to as B3 to B10 from trigonal to decagonal, whereas the corresponding single tubes (either the inner or outer tube of the double tube) are denoted as P3 to P10.
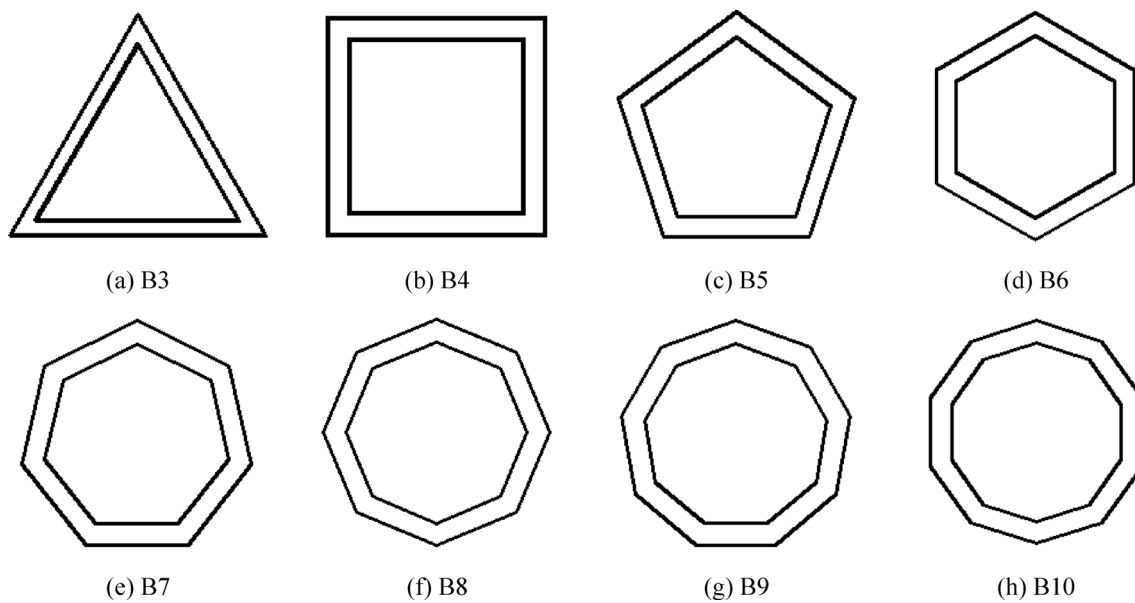
(a) B3　　　　(b) B4　　　　(c) B5　　　　(d) B6

(e) B7　　　　(f) B8　　　　(g) B9　　　　(h) B10

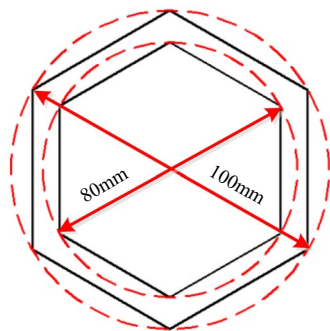**Fig. 1** Cross-sectional shapes of different polygonal double-tube structures

Fig. 2 Circumscribed circle diameter of inner and outer tube of polygonal double-tube structures
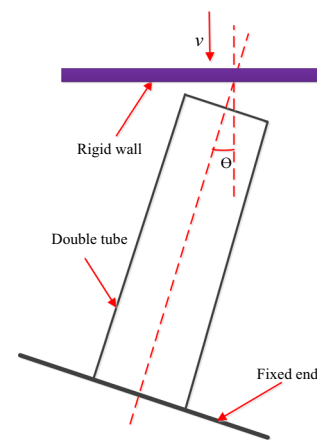

Fig. 3 Finite element boundary conditions of double tube under multiple angle loads

3 Finite element model and validation

3.1 Finite element modeling

Figure 3 depicts the boundary conditions of the finite element model for the double tubes when subjected to a variety of angle loads. This article focuses primarily on researching the energy absorption characteristics of polygonal double tubes under oblique loadings at 0°, 10°, 20°, and 30° (Sun et al. 2018; Gao et al. 2016b, a). Figure 4 shows a finite element model of the double tubes under multiple angle loadings. The 4-node Belytschko-Tsay reduced integration shell elements are used to simulate the crushing behaviors of the thin-walled structure. Under the condition of ensuring calculation accuracy, shell element sizes have been determined to be 2.0×2.0 mm.

Single-surface contact is employed to account for the contact of the double tube itself during the crushing process, and node-to-surface contact is utilized to replicate the contact between the rigid plate and the double tube. As reported in Ref. (Li et al. 2020), the dynamic and static friction coefficients were considered to be 0.2 and 0.3, respectively, for the contact parameters that are a part of the computation for the numerical simulation. The MAT24 material model in LS-DYNA is used to characterize the mechanical behavior of aluminum materials. Because aluminum is a material that is not sensitive to strain rate, the influence of strain rate can
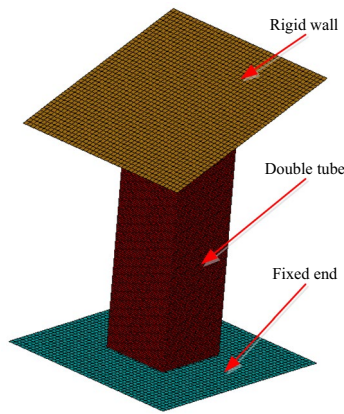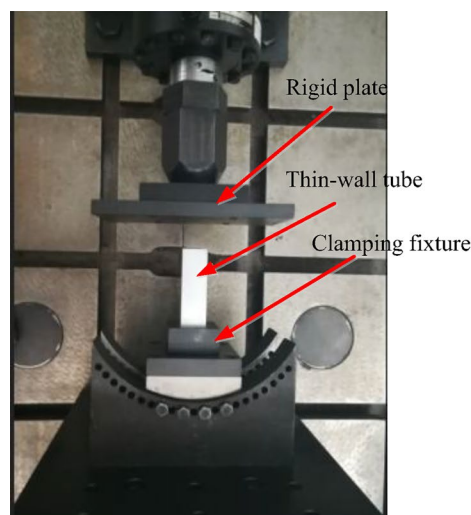
Fig. 4 Finite element model of double tube under multiple angle loads

be neglected while performing numerical simulations (Fang et al. 2015). The velocity of the impact load is 10 m/s, and the additional mass of the rigid wall is 600 kg (Ying et al. 2017).

3.2 Model validation

The quasi-static axial crushing test of thin-walled square tubes is performed using an MTS testing machine designed with a load capacity of 50 kN, as illustrated in Fig. 5. The specifications of the square tubes are 120 mm in length, 30 mm in width, and 1 mm in wall thickness. The square tube sample is positioned on the fixed base plate via a specially designed fixture, comprising two blocks with a 1 mm gap. The fixture permitted clamping of the sample within the gap. The loading is applied to the free end of the sample via a rigid plate attached to the actuator and a load cell. The loading to each sample is applied at a rate of 10 mm/min. The time histories of force and deflection signals along the axial direction are acquired for subsequent analyses.

The validity of the finite element model is examined by comparing the measured deformation patterns and force response of the square tube with those obtained from the finite element model. Figure 6 presents the deformed pictorial views of square tubes obtained from the measurements and numerical simulations following the quasi-static axial loading. The measured and simulated deformation patterns exhibit reasonably good agreements in terms of the deformation modes and the number of folding lobes of the square tubes under axial loading.

Figure 7 shows the force–displacement response curves of square tubes derived from measurements and numerical simulations under axial loading. Table 1 provides a summary of the magnitudes of the initial force peaks and the corresponding mean forces that are determined from the
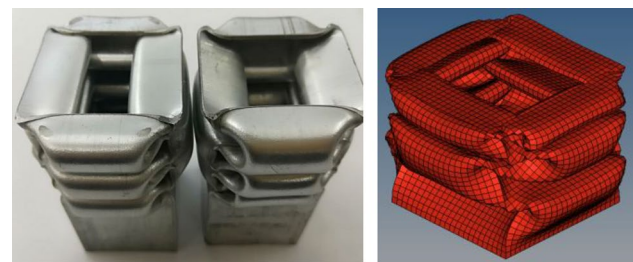
(a) Experiment   (b) Simulation

Fig. 6 Deformation patterns of square tube under axial loading

Fig. 5 axial crushing test of thin-walled square tube
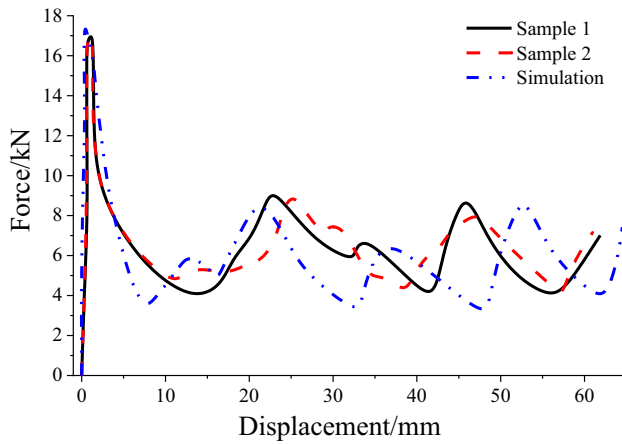

(a) Axial load   (b) Square tube sample

Fig. 7 Fore–displacement curves of square tube under axial loading

simulations and experiments for the square tubes when they are subjected to axial loading. The findings demonstrate extremely high agreements between the initial peak force and the mean force. The relative errors in peak and mean forces are less than 4% and 8%, respectively, for the square tube structures. According to the comparisons shown in Figs. 6 and 7, as well as Table 1, it can be deduced that the finite element model is capable of providing reasonably accurate estimations of the crush responses of thin-walled square tubes subjected to axial loading. In addition, the above-described finite element model can be applied to the upcoming oblique loading analysis of double-tube structures (Chen et al. 2017; Tran and Baroutaji 2018).

4 Crushing performances of single and double tubes

4.1 Comparison of triangular single and double tubes

As shown in Fig. 8, the numerical simulation is initially performed to evaluate the crushing characteristics of the triangular single and double tubes under multiple loading angles, including force–displacement curves of single and double tubes as well as those of the sum of the crushing loads for the inner and outer tubes. The illustration

demonstrates that the initial peak force of the double tubes is more significant than that of the single tubes and is almost equal to the sum of the initial peak forces of the inner and outer tubes.

Table 2 displays the energy absorbed by the triangular single and double tubes at different loading angles, as well as the sum of the energy absorbed when the inner and outer tubes are loaded independently. When loaded axially as well as obliquely at 10°, the energy absorbed by the double tube is more than the sum of the energy absorbed by the inner and outer tubes loaded individually. As a result of the interaction between the inner and outer tubes of triangular double tubes, the energy absorption capacity of the double tubes increases by 3.34% and 7.57%, respectively, for these loading conditions at 0 and 10°. Under oblique loading at 10°, the energy-absorbing capacity is substantially increased, and the interaction between the inner and outer tubes is more noticeable than it is under axial loading. When subjected to oblique loading at angles of 20° and 30°, the energy absorbed by the double tubes is less than the sum of the energy absorbed by the inner and outer tubes loaded independently, and this difference between them will continue to rise as the loading angle is increased.

When comparing the crushing capacities of the triangular single and double tubes, the specific energy absorption is used as the metric because of the significant difference in mass between the two types of tubes. The double tubes, in contrast to the single tubes, have a higher specific energy absorption at loading angles of 0° and 10° as well as 20°, as shown in Table 3. The increases in specific energy absorption for the three different angles are 6.77%, 13.62%, and 2.97%, respectively. On the contrary, the specific energy absorption of the double tubes for oblique loading at 30° is reduced by 22.34% compared to that of the single tubes. While both the single and double tubes display global bending deformation, the latter is more susceptible to the effects of loads in excess of the critical load angle.

In conclusion, in addition to large-angle oblique loadings, the space utilization rate, energy absorption capacity, and specific energy absorption of the triangular single tubes may all be improved by inserting a hollow tube within them. The energy absorption properties under

Table 1 Comparisons of initial peak force (F_{max}) and corresponding mean force (F_{mean}) magnitudes obtained from experiments and simulations of the square tubes under axial loading

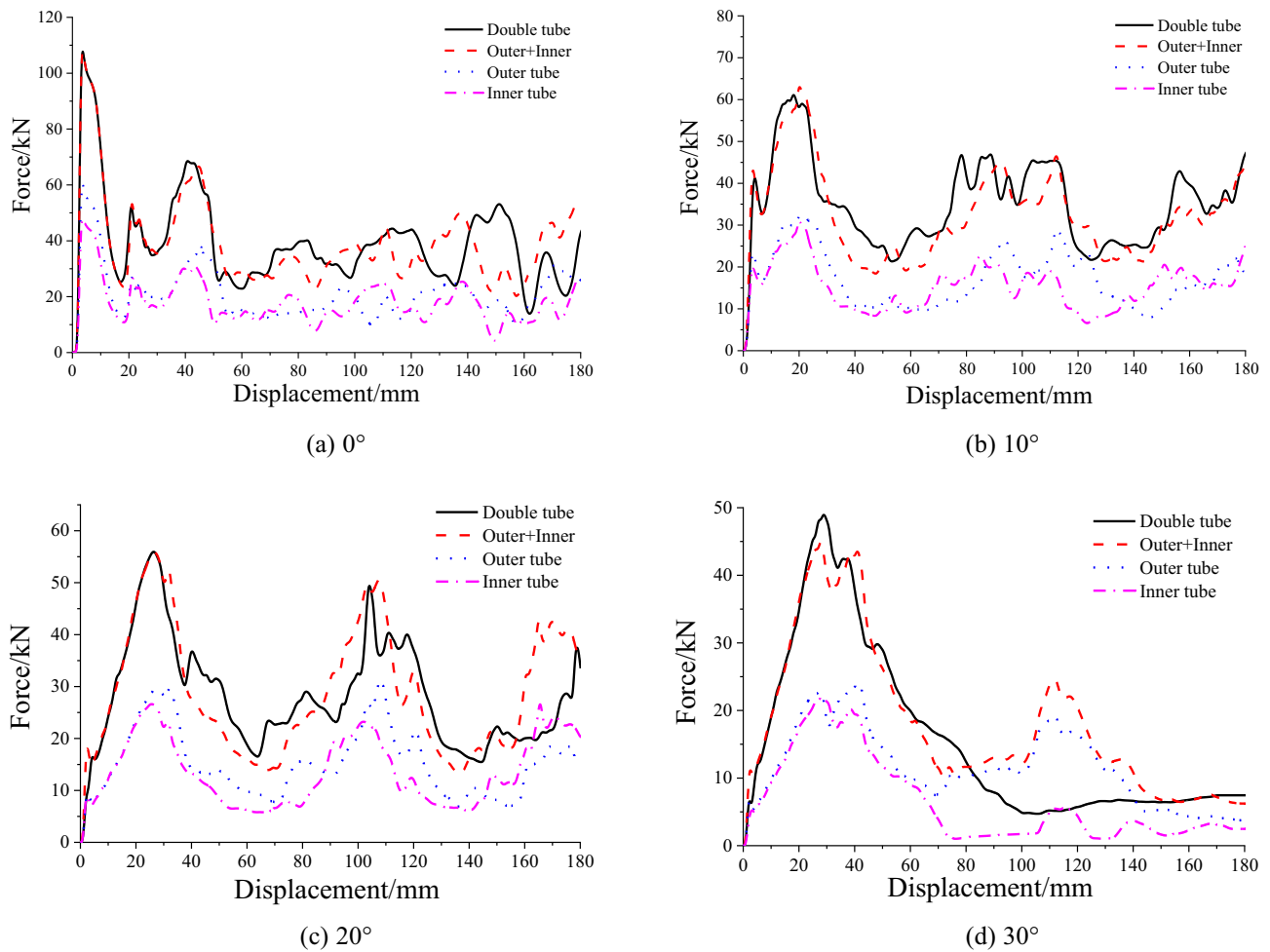|	Experiment/kN		Simulation/kN		Relative error /%	
	F_{max}	F_{mean}	F_{max}	F_{mean}	F_{max}	F_{mean}
Sample 1	17.06	6.19	17.75	5.93	3.89	4.38
Sample 2	17.25	6.35	17.75	5.93	2.82	7.08

(a) 0°

(b) 10°

(c) 20°

(d) 30°

Fig. 8 Crushing force–displacement curves of triangular single and double tubes under multiple angle loading

Table 2 Energy absorption capacity of triangular single and double tubes under multiple angle loading

	E/J			
	0°	10°	20°	30°
Outer tube	3279	2620	2265	1584
Inner tube	2821	2359	1970	855
Outer + Inner	6100	4979	4235	2439
Double tube (B3)	6304	5356	4200	2214

Table 3 Specific energy absorption of triangular single and double tubes under multiple angle loading

	SEA/J/g			
	0°	10°	20°	30°
Outer tube	9.74	7.78	6.73	4.70
Inner tube	10.47	8.76	7.31	3.17
Outer + Inner	10.06	8.21	6.99	4.02
Double tube (B3)	10.40	8.84	6.93	3.65

axial and small-angle oblique loads may be significantly improved by using double tubes instead of single ones.

4.2 Comparison of polygonal single and double tubes

The deformation patterns of polygonal single and double tubes with various cross-sectional forms that are subjected to multiple loading angles are shown in Tables 4 and 5, respectively. Polygonal single and double tubes show a progressive collapse pattern with high and steady energy absorption response when loads at 0° and 10° are applied. When the loading angle is increased to 20°, the progressive collapse pattern is still exhibited by the triangular, quadrilateral, and pentagonal single and double tubes, while the other polygonal tubes show a global bending deformation, and their energy absorption capacity decreases. All single and double tubes undergo varying degrees of global bending deformation at a loading angle of 30°.

Table 4 Crushing deformation patterns of polygonal single tubes (outer tube) under multiple angle loadings
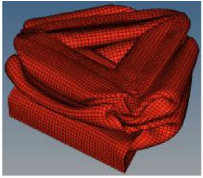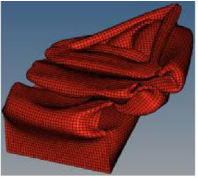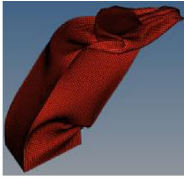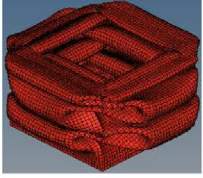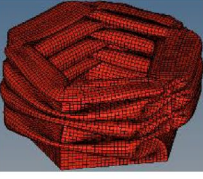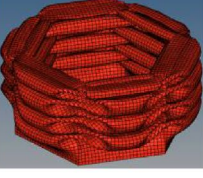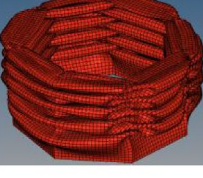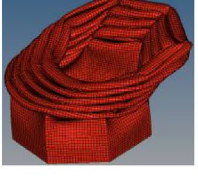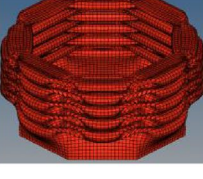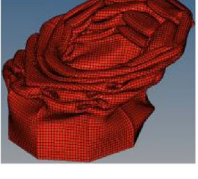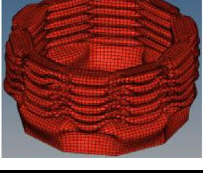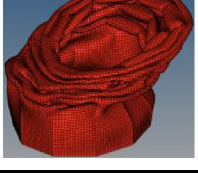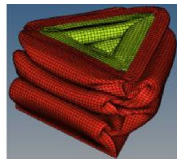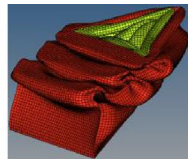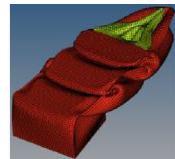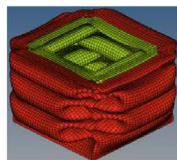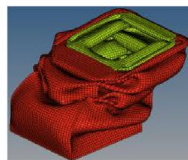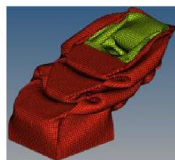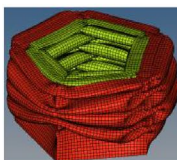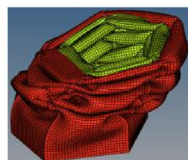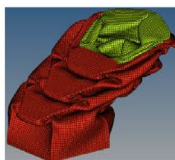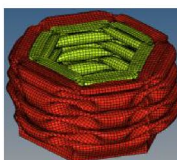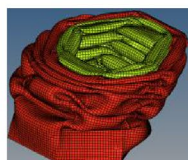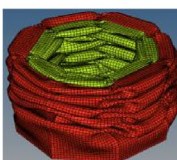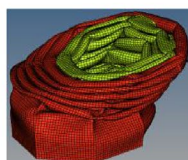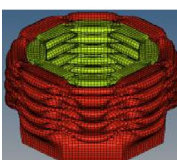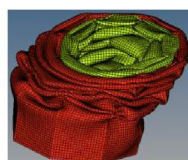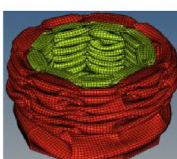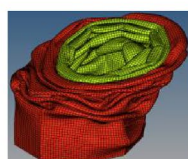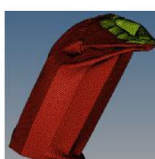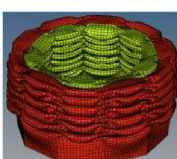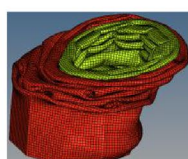
Model	0°	10°	20°	30°
P3				
P4				
P5				
P6				
P7				
P8				
P9				
P10				

Table 5 Crushing deformation patterns of polygonal double tubes under multiple angle loadings

Model	0°	10°	20°	30°
B3				
B4				
B5				
B6				
B7				
B8				
B9				
B10				

There are several distinctions between the single and double tubes although the fact that their crushing patterns under oblique loading at large angles are identical. Compared with the outer tube of the double-tube structures, the folded lobes produced by the single tubes prior to the global bending deformation are more. The single tubes have a higher energy

absorption efficiency since more materials are involved in the process.

As can be shown in Tables 4 and 5, the critical loading angles for the triangular, quadrilateral, and pentagonal single and double tubes fall within the range of 20° to 30°, whereas those for the other polygonal structures fall within the range of 10° to 20°. While both single and double tubes have similar critical loading angles, the energy absorption efficiency of the former is greater because more material is involved in absorbing impact energy prior to developing global bending deformation. Therefore, it is crucial for the practical application of double-tube structures to make improvements to the energy absorption properties under oblique loading, particularly at large angles.

Figure 9 shows the energy absorption capacity of the polygonal single and double tubes under different loading angles. This graphic shows that the energy absorption capacity of the polygonal double tubes under these loading conditions (0 and 10°) is higher than the sum of the energy absorbed when the inner and outer tubes are loaded independently. It demonstrates that the inner and outer tubes of the double tubes interact during the crushing deformation

process when subjected to axial and small-angle oblique loadings; however, the degree of interaction between the inner and outer tubes varies depending on the cross-sectional shapes of the double tubes.

Only the energy absorption capacity of the pentagonal double tubes is higher than the sum of the energy absorbed by the inner and outer loaded independently when the loading angle is increased up to 20°. The reason for this is that the progressive crushing deformation produced by the pentagonal double tubes cannot be achieved by the inner and outer tubes loaded independently. The energy absorption capacity of the triangular and quadrilateral double tubes is somewhat smaller than the total energy absorbed when their inner and outer tubes are loaded independently. At this loading angle, both single and double tubes experience progressive collapse deformation, and the loading angle is to blame for the decreased energy absorption capacity. The global bending deformation takes place from the hexagonal to decagonal double tubes, which results in a significant decrease in the energy absorption capacity. This reduction is even more significant than the total energy absorption reduction when the inner and outer tubes are loaded

(a) 0°

(b) 10°

(c) 20°

(d) 30°
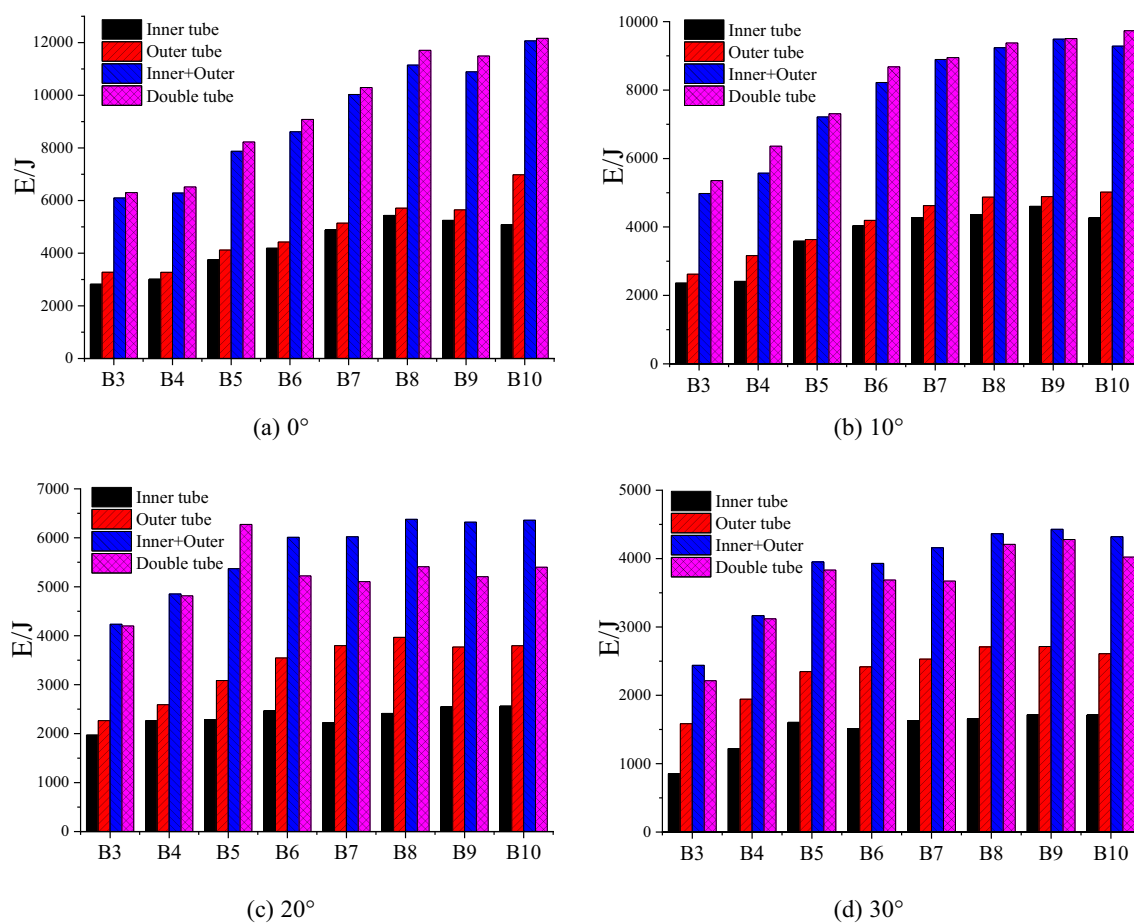
Fig. 9 Energy absorption capacity of polygonal single and double tubes under different loading angles

independently, reaching a maximum of 17.63%. All the double tubes experience global bending deformation when loaded at 30°. Their energy absorption capacity is lower than the sum of the energy absorbed by their inner and outer tubes loaded independently, and the maximum difference between these two capacities is 11.71%.

When a global bending deformation occurs, relative to an axial load, the energy absorption capacity of the polygonal single (outer tube) and double tubes reduces by 19.86%-51.69% and 42.51%-64.88%, respectively, as demonstrated in Fig. 9. The double tubes are more impacted by the loading angles, and their energy absorption capacity decreases more significantly. Therefore, it is of great significance to raise the critical loading angle of the double tubes in order to optimize their oblique energy absorption properties.

The specific energy absorption of the single (outer tube) and double tubes under varying loading angles is shown in Fig. 10. The figure demonstrates that, except for the decagonal double tube, all the other double tubes have larger specific energy absorption than the single ones under axial and 10° oblique loading. When the loading angle is raised

to 20°, the triangular, quadrilateral, and pentagonal double tubes have a better specific energy absorption than the single tubes. However, the specific energy absorption of the other polygonal double tubes is between 18.19% and 25.31% lower than that of the single tubes. Increasing the loading angle to 30°, the polygonal double tubes have a lower specific energy absorption than the single tubes, with a maximum difference of 22.34% between the single- and double-tube configurations.

To summarize, adopting the double tubes may enhance the space utilization rate and energy absorption characteristics under axial and small-angle oblique loads owing to the interaction between the inner and outer tubes during crushing deformation. However, when the oblique loading angle is increased beyond the critical loading angle that causes the global bending deformation, the double tubes are more affected by the loading angle, and their energy absorption capacity and specific energy absorption decrease significantly. Furthermore, their energy absorption characteristics are even worse than those of the single tubes.
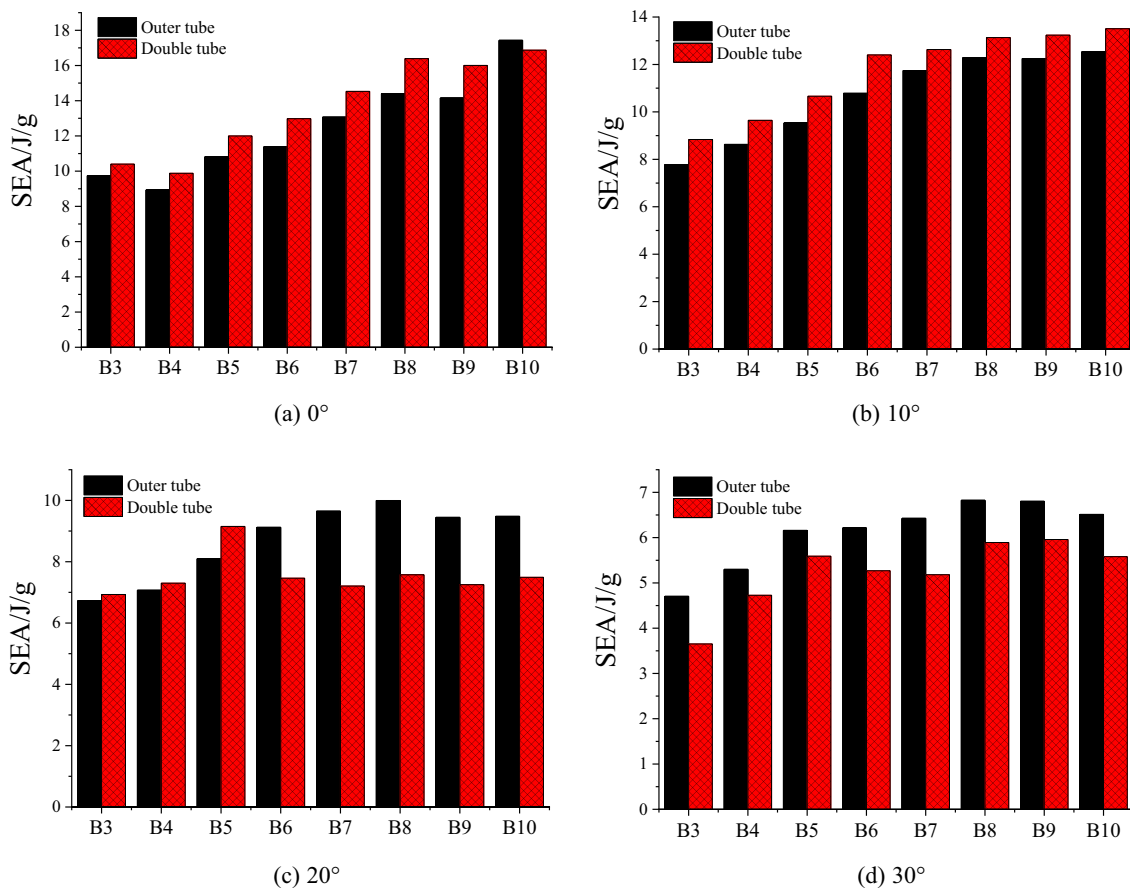
Fig. 10 Specific energy absorption of single and double tubes under different loading angles

4.3 Energy absorption characteristics of double tubes

The energy absorption characteristics of polygonal double tubes with various cross-sectional forms under different loading angles are shown in Fig. 11. The graphic demonstrates how the loading angle impacts the double tubes' capacity to absorb energy. As the loading angle increases, the double tubes experience a decrease in their initial peak force, mean load, and specific energy absorption to varying degrees. For axial and 10° oblique loads, the mean load and specific energy absorption of the polygonal double tubes rise as the number of sides increases. The reason is that the number of plastic hinge lines and folded lobes created rises as the number of sides grows. When the loading angle is raised to 20° and 30°, the double tubes with more edges are more susceptible to occurring global bending deformation. At the same time, the number of folded lobes and the amount of material used to absorb energy in the double tubes reduce. The reason is that as the number of sides increases, the cross-sectional perimeter and the number of corner elements for the polygonal tubes rise. It means more force is needed to make the plastic hinge lines and the folded lobes.

The force easily surpasses the load necessary to produce a global bending deformation, resulting in the global bending deformation of the double tubes.

The number of sides of polygonal double tubes also has an effect on the initial peak force and crushing force efficiency. When subjected to axial loading, the initial peak force and crushing force efficiency of the polygonal double tubes rise with an increase in the number of sides. When subjected to oblique loading, their initial peak force and crushing force efficiency decrease as the loading angle increases.

5 Evaluation of comprehensive performances of double tubes

5.1 Grey relational analysis (GRA)

The basic idea of grey relational analysis (GRA) is to determine the optimal design scheme by calculating the correlation degree between different design cases and the ideal one. This technique may also comprehensively take into account multiple performance indices and reasonably evaluate the

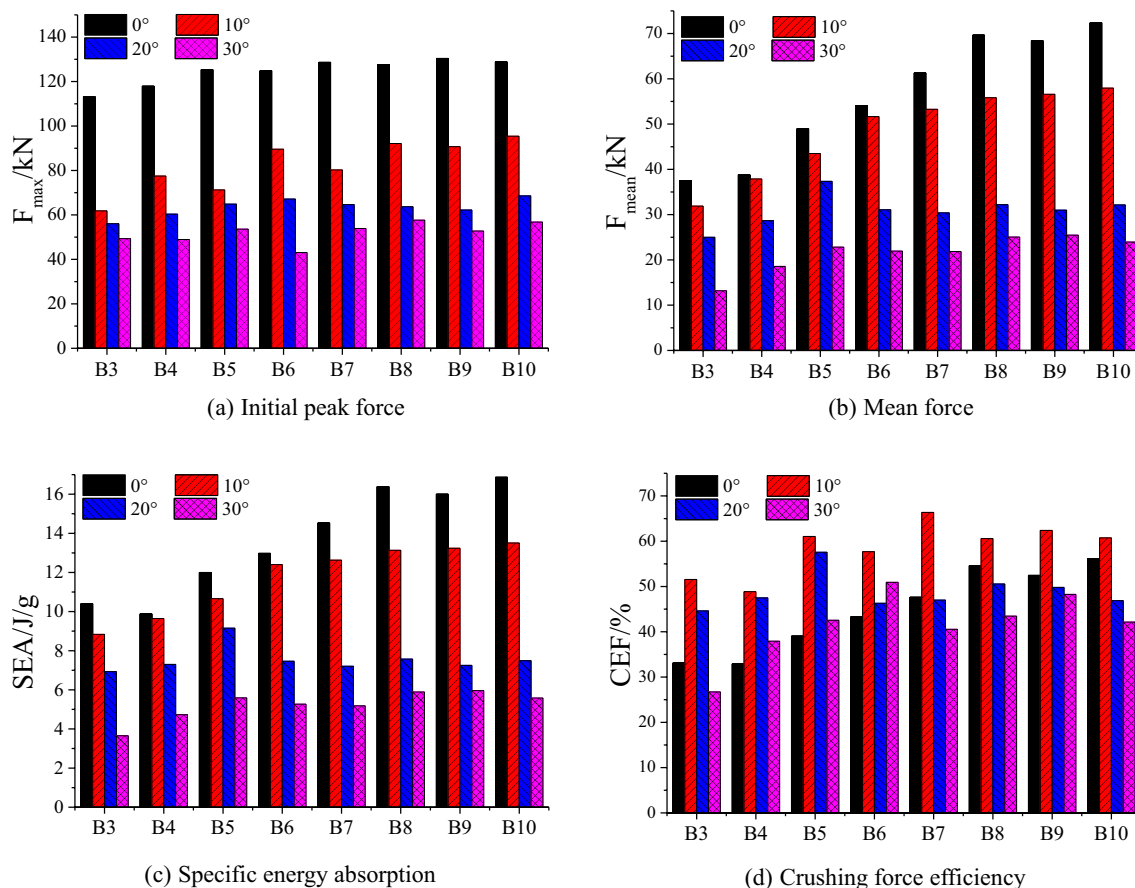(a) Initial peak force (b) Mean force (c) Specific energy absorption (d) Crushing force efficiency

Fig. 11 Energy absorption characteristics of polygonal double tubes under different loading angles

comprehensive energy absorption characteristics of thin-walled structures subjected to different angle loadings (Xiong et al. 2018).

The following is the calculation processes for selecting the optimal design strategy using grey relational analysis:

Step 1: Define the initial decision-making matrix **X**:

$$X = \left[x_i(k) \right]_{mn} = \begin{bmatrix} x_1(1) & x_1(2) & \cdots & x_1(n) \\ x_2(1) & x_2(2) & \cdots & x_2(n) \\ \vdots & \vdots & \vdots & \vdots \\ x_m(1) & x_m(2) & \cdots & x_m(n) \end{bmatrix} \tag{1}$$

where $x_i(k)$ is the performance value of the ith design case with respect to the kth performance criterion. The subscripts m and n refer to the number of design cases and performance criteria, respectively.

Step 2: Normalize the initial decision-making matrix to yield a non-dimensional matrix:

Distinct units and values of performance criteria in the first decision-making matrix make it challenging to compare different criteria concerning the various design cases. Normalizing the initial decision-making matrix is necessary before beginning grey relational analysis (GRA).

Dimensionless treatment of positive criteria:

$$x_i(k)^* = \frac{x_i(k) - \min(x_i(k), i = 1, 2, \cdots, m)}{\max\left(x_i(k), i = 1, 2, \cdots, m\right) - \min(x_i(k), i = 1, 2, \cdots, m)}$$
$$(k = 1, 2, \cdots, n \tag{2}$$

Dimensionless treatment of negative criteria:

$$x_i(k)^* = \frac{x_i(k) - \max(x_i(k), i = 1, 2, \cdots, m)}{\min\left(x_i(k), i = 1, 2, \cdots, m\right) - \max(x_i(k), i = 1, 2, \cdots, m)}$$
$$(k = 1, 2, \cdots, n) \tag{3}$$

Step 3: Determine the reference sequence, which is an ideal design scheme that is produced by the optimal value of each performance criterion in the non-dimensional matrix:

$$X^* = \left(x_0(1)^*, x_0(2)^*, \cdots, x_0(n)^*\right) = \left(Optimum\left(x_i(k)^*, i = 1, 2, \cdots, m\right),\right.$$
$$k = 1, 2, \cdots, n)$$
$$\tag{4}$$

Step 4: Calculate the grey relational coefficient between various design cases and the ideal case:

$$\xi_i(k) = \frac{\displaystyle\min_{\forall i}\min_{\forall k}\left|x_0(k)^* - x_i(k)^*\right| + \rho \cdot \max_{\forall i}\max_{\forall k}\left|x_0(k)^* - x_i(k)^*\right|}{\left|x_0(k)^* - x_i(k)^*\right| + \rho \cdot \max_{\forall i}\max_{\forall k}\left|x_0(k)^* - x_i(k)^*\right|} \tag{5}$$

where ρ is the resolution coefficient with a range of [0,1] and a typical value of 0.5.

Step 5: Calculate the grey relational degree:

After determining the relational coefficient between specific design cases and the ideal case, the grey relational degree can be calculated as follows:

$$\gamma_i = \frac{1}{n} \sum_{k=1}^{n} \xi_i(k) \tag{6}$$

It is required to apply distinct weight factors due to the different importance of each performance criterion in practical application. The following is the calculation equation for the grey relational degree:

$$\gamma_i = \sum_{k=1}^{n} w_k \cdot \xi_i(k) \quad \sum_{k=1}^{n} w_k = 1 \tag{7}$$

where w_k represents the weight factor of the kth performance criterion.

The combination weighting method is adopted to calculate the weight coefficient for each performance criterion (Du et al. 2011), which comprehensively considers the influence of subjective and objective factors on the weight coefficient. The calculation expression is as follows:

$$w_k = \frac{\alpha_k \beta_k}{\sum_{k=1}^{n} \alpha_k \beta_k} \tag{8}$$

where α_k is the subjective weight of each performance criterion derived by comparing two distinct criteria, as reported in Ref. (Li et al. 2019); β_k is the objective weight of each performance criterion computed using the entropy weight technique. Table 6 presents the values of w_k.

5.2 Determination of the optimal double tubes

Table 6 summarizes the energy-absorbing properties of eight polygonal double tubes subjected to varying loading angles. The grey relational analysis (GRA) is used to evaluate the comprehensive energy absorption characteristics of the double tubes. The optimal polygonal double tubes are determined based on the relational degree values between the various design cases and the ideal case (reference sequence). It is clear from Table 7 that the B9 double tubes exhibit the best comprehensive crushing performance when subjected to various loading angles.

6 Crushing behaviors and optimization of FGT double tubes

In comparison to single tubes, polygonal double tubes have a bigger energy absorption capacity as well as a higher specific energy absorption when subjected to axial and small-angle oblique loadings. It is shown by the findings of

Table 6 Energy absorption characteristics and weight coefficients of double tubes under different loading angles

Indices	Angle	B3	B4	B5	B6	B7	B8	B9	B10	w_k
F_{max}/kN	0°	113.19	117.93	125.38	124.88	128.64	127.59	130.39	128.86	0.0699
	10°	61.83	77.51	71.25	89.55	80.26	92.15	90.69	95.42	0.0707
	20°	56.03	60.37	64.87	67.15	64.66	63.68	62.23	68.57	0.0670
	30°	49.33	48.95	53.63	43.10	53.89	57.64	52.77	56.81	0.0702
F_{mean}/kN	0°	37.52	38.81	48.98	54.06	61.28	69.68	68.40	72.39	0.0725
	10°	31.88	37.87	43.50	51.66	53.27	55.82	56.58	57.95	0.0716
	20°	25.00	28.67	37.34	31.08	30.39	32.20	30.99	32.14	0.0703
	30°	13.18	18.56	22.81	21.95	21.85	25.05	25.47	23.94	0.0715
SAE/J/g	0°	10.40	9.88	12.00	12.98	14.53	16.39	16.00	16.87	0.0716
	10°	8.84	9.64	10.66	12.40	12.63	13.13	13.24	13.50	0.0709
	20°	6.93	7.30	9.15	7.46	7.21	7.57	7.25	7.49	0.0701
	30°	3.65	4.73	5.59	5.27	5.18	5.89	5.96	5.58	0.0708
CFE/%	0°	33.15	32.91	39.06	43.29	47.64	54.61	52.46	56.18	0.0380
	10°	51.56	48.88	61.05	57.69	66.37	60.58	62.38	60.73	0.0372
	20°	44.62	47.48	57.57	46.29	47.00	50.56	49.80	46.87	0.0371
	30°	26.71	37.93	42.54	50.92	40.55	43.45	48.27	42.14	0.0377

Table 7 Comprehensive performance rank of polygonal double tubes under different multiple angle loading

`	B3	B4	B5	B6	B7	B8	**B9**	B10
Relational degree	0.4908	0.4465	0.6005	0.5576	0.5471	0.6526	**0.6641**	0.6557
Rank	7	8	4	5	6	3	**1**	2

The bold is used to indicate that this value is maximum. The greater the value, the better the crushing performance of the double-tubes structure. So, B9 tube has the best comprehensive crushing performance under various loading angles

the study presented above. Due to the interaction between the inner and outer tubes during the crushing deformation process, the energy absorption capacity of the double tubes is greater than the sum of the energy absorbed by the inner and outer tubes when loaded separately. However, the double tubes are more likely to experience global bending deformation when subjected to oblique loadings at large angles. This leads to a significant reduction in the energy absorption characteristics of the structures, which is even worse than those of the single tubes. For this reason, this subsection aims to enhance the energy absorption characteristics of the double tubes under large-angle oblique loadings by increasing their critical loading angle.

6.1 Crushing performances of FGT double tubes

Figure 12 is a schematic diagram of a thin-wall structure with a functionally graded thickness (FGT). The tube's thickness is varying along its axial direction. The following Equation (Fang et al. 2016) may be used to calculate the wall thickness at various locations:

Fig. 12 a FGT thin-wall structure
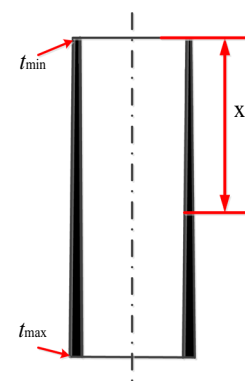
$$t(x) = t_{min} + (t_{max} - t_{min}) \times \left(\frac{x}{L}\right)^{10^m} \tag{9}$$

where t_{min} and t_{max} are the minimum and maximum thicknesses, respectively. x is the distance shown in Fig. 12. L is the length of the FGT tube. m denotes the gradient parameter that governs the thickness variation, as shown in Fig. 13.

According to the investigation findings presented in Sect. 4.2, the B9 double tube has the most comprehensive crushing performance for four kinds of loading angles. As a result, the FGT structural study is mostly centered on the
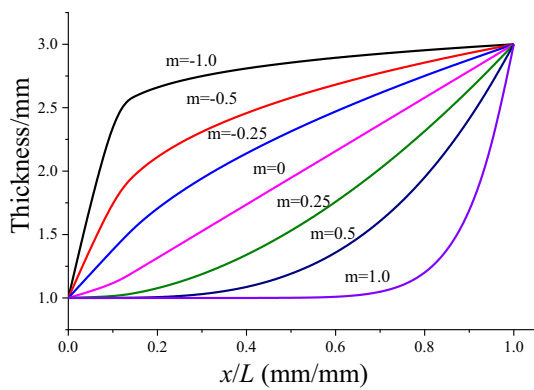
Fig. 13 Effects of the gradient parameters on wall thickness

B9 double tube. For the FGT double tube, the gradient indices of the inner and outer tubes are 0, their minimum and maximum thicknesses are 1 mm and 3 mm, respectively, and their length is 240 mm. It allows for a direct comparison of the crushing performances of the FGT and uniform thickness (UT) B9 double tubes. There is currently no discernible mass difference between the FGT and UT B9 double tubes.

Figure 14 depicts the crushing deformation patterns of the FGT B9 double tube under various loading angles. The double tube exhibits a gradual collapse deformation for four loading angles without undergoing a global bending, as observed in the graphic. Table 5 shows that the critical loading angle for a UT B9 double tube falls between 10° and 20°, whereas that for a FGT B9 tube is larger than 30°. Therefore, adopting varying thickness instead of uniform one can enhance the critical loading angle and energy absorption characteristic of B9 double-tube multiple angle loads.

Table 8 shows that under oblique loading at large angles, the FGT double tube has a better energy absorption capacity and a much lower initial peak force than the UT double one. Under axial and 10° oblique loading, however, the energy absorption capacity of the FGT double tube is decreased by 22.96% and 6.88%, respectively, compared with the UT double one. Although the UT and FGT double tubes exhibit a progressive collapse deformation under axial and small-angle oblique loading, the FGT double ones have fewer materials participating in energy absorption.

In conclusion, the critical loading angle and oblique energy absorption characteristics of the B9 double tube can be improved by adapting the FGT structure to replace the uniform thickness one. However, the structural parameters (m, t_{min} and t_{max}) need to be reasonably selected; otherwise, the energy absorption capacity of the double tubes under axial and small-angle oblique loadings may be greatly reduced.

6.2 Parameter analysis

For the FGT B9 double tube, the parameters that affect its energy absorption characteristics include the gradient index m that controls the change in the thickness of the inner and outer tubes and the minimum thicknesses of the inner and outer tubes. When used for parameter analysis, the B9 double tube has the following specifications: the gradient indices m for the inner and outer tubes are equal to 0, and the minimum and maximum thicknesses for the inner and outer tubes, respectively, are 1 mm and 3 mm, as well as the tubes' length is 240 mm.
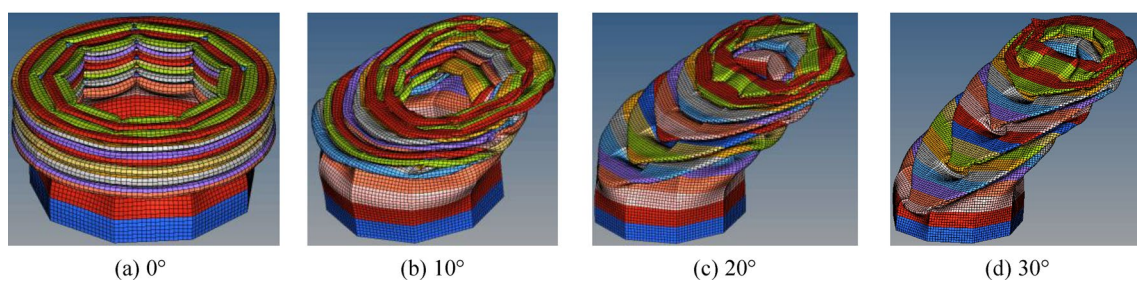
Fig. 14 Crushing deformation patterns of the FGT B9 double tube under different loading angles

Table 8 Crushing performances of uniform thickness and FGT B9 double tubes under different loading angles

	F_{max}/kN				E/J			
	0°	10°	20°	30°	0°	10°	20°	30°
Uniform thickness	130.39	90.69	62.23	52.77	11,492	9505	5206	4279
FGT	71.70	32.54	45.49	45.41	8853	8852	7329	5939
Relative variation /%	− 45.01	− 64.12	− 26.90	− 13.95	− 22.96	− 6.87	40.78	38.79

6.2.1 Gradient index *m* of inner tube

The only structural parameter that is altered is the gradient index *m* governing the inner tube thickness. The effect of the gradient index *m* on the energy absorption properties of the FGT double tube is investigated. Crushing performance curves of the FGT double tube with various gradient indices under varying loading angles are generated by selecting *m* at a fixed interval ($m = -1.0$, -0.5, 0.0, 0.5, and 1.0), as shown in Fig. 15. It is evident that decreasing the gradient index results in both the energy absorption capacity of the double tube as well as its specific energy absorption. However, the gradient index cannot be constantly lowered because this could cause the double tube to undergo global bending deformation under oblique loading at large angles, leading to a significant reduction in both its energy absorption capacity and specific energy absorption.
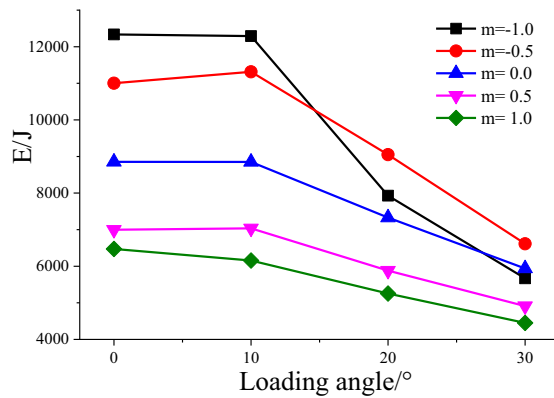
6.2.2 Minimum thickness of inner tube

The impact of the minimum thickness for the inner tube on the energy absorption properties of the FGT double tube is explored by changing the minimum thickness of the inner tube while maintaining the other structural parameters in their original states. The inner tube has minimum thicknesses of 1.0 mm, 1.5 mm, 2.0 mm, and 2.5 mm, respectively. The influence of various minimum thicknesses on the energy absorption capacity and specific energy absorption of the double tube is shown in Fig. 16. As the picture demonstrates, the energy absorption properties of the double tube under multiple loading angles may be optimized by adjusting the minimum thickness of its inner tube. However, the minimum thickness for the inner tube should not be too great. Under oblique loading at large angles, an excessive value for the minimum thickness will result in a considerable decrease in the energy absorption capacity and specific energy absorption of the double tube.

(a) Energy absorption capacity
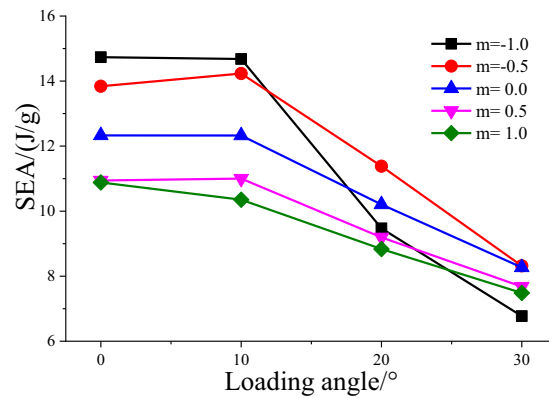
(b) Specific energy absorption

Fig. 15 Effects of gradient index of inner tube on energy absorption characteristics

(a) Energy absorption capacity

(b) Specific energy absorption

Fig. 16 Effects of minimum thickness of inner tube on energy absorption characteristics

6.2.3 Gradient index *m* of outer tube

The effect of the gradient index *m* for the outer tube thickness on the energy absorption properties of the FGT double tube is investigated by varying the gradient value controlling the thickness variation law while maintaining all other structural parameters at their default states. The gradient values are specified as − 1.0, − 0.5, 0, 0.5, and 1.0, in that sequence, for the outer tube thickness. It is clear from examining Fig. 17 that lowering the gradient value results in an increase in the energy absorption capacity of the double tube under different angle loadings. However, a decrease in gradient value is not necessarily accompanied by an increase in its specific energy absorption.
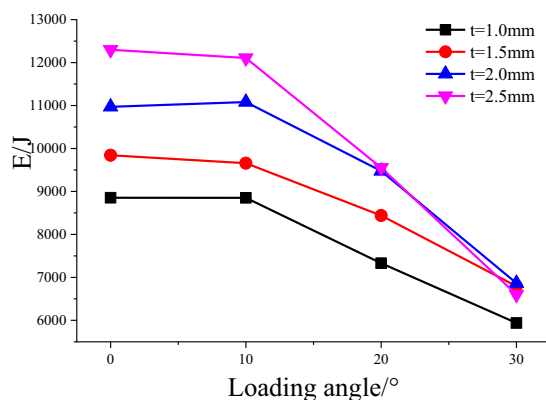
6.2.4 Minimum thickness of outer tube

The influence of the minimum thickness for the outer tube on the energy absorption characteristics of the FGT double tube is studied, with the exception that the minimum thickness is the only parameter that is altered in this study. Other structural parameters are left unaltered. The minimum thicknesses are set to -1.0, -0.5, 0, 0.5, and 1.0, respectively, for the outer tube. Figure 18 shows that when the minimum thickness of the outer tube is less than or equal to 2.0 mm, the energy absorption capacity and specific energy absorption of the double tube increase as the minimum thickness increases. However, as the minimum thickness increases to 2.5 mm, the excessive thickness will result in a significant decrease in the energy absorption capacity and specific energy absorption of the double tube under 30° oblique loading.

To summarize, the energy absorption characteristics of the FGT double tube are significantly influenced by the gradient index and the minimum thickness of the inner and outer tubes. Energy absorption characteristics of the double tube are dramatically diminished under oblique loading at large angles if the essential parameters are not selected

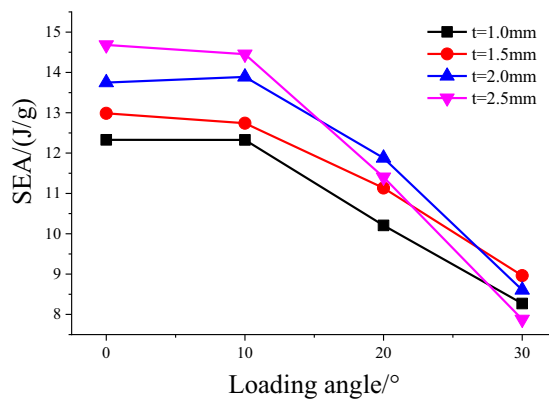(a) Energy absorption capacity

(b) Specific energy absorption
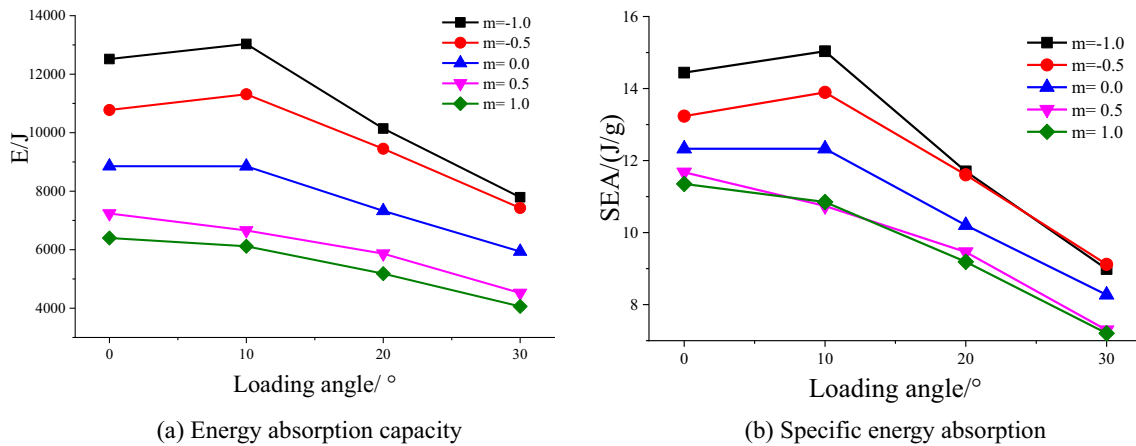
Fig. 17 Effects of gradient index of outer tube on energy absorption characteristics

(a) Energy absorption capacity
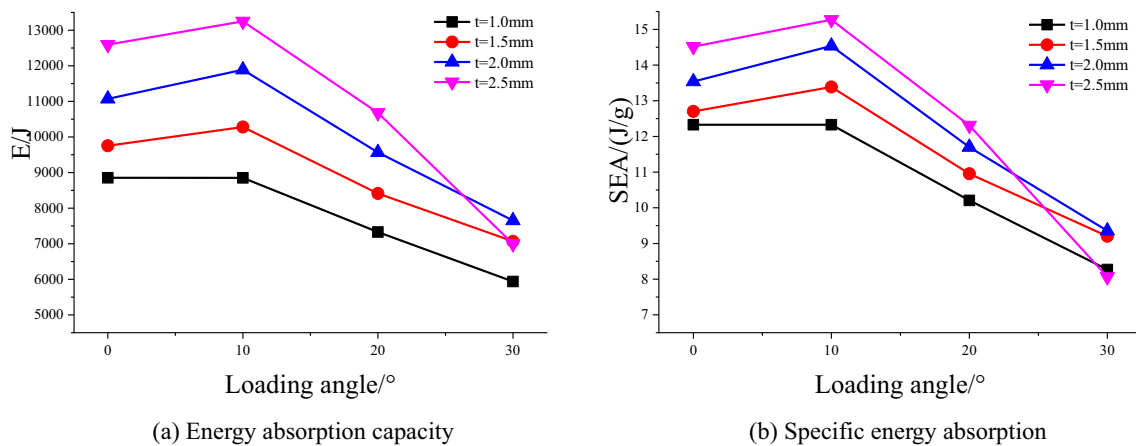
(b) Specific energy absorption

Fig. 18 Effects of minimum thickness of outer tube on energy absorption characteristics

sensibly. Because of this, for the double tube to demonstrate superior crushing performance under various loading angles, it is crucial to set values for each parameter sensibly in accordance with the optimization design approach.

6.3 Crashworthiness optimization of FGT double tube

6.3.1 Design of experiment

For the FGT B9 double tube, the structural parameters affecting the crushing performance are the gradient index and minimum thickness of the inner and outer tubes. The gradient index and minimum thickness are within the ranges of $[-1, 1]$ and $[1.0\,\text{mm}, 2.5\,\text{mm}]$, respectively. As indicated in Table 9, the four parameters are employed as design variables, and 25 sample points are determined by the optimal Latin hypercube sampling technique, and the response values of the related models are then calculated. The overall mass of the double tube is denoted by M, while its comprehensive energy absorption capacity and maximum initial peak force, respectively, are denoted by E^θ and $F^\theta_{\max}$. The following are the calculation expressions for E^θ and $F^\theta_{\max}$:

$$E^\theta = \sum_{i=1}^{n} w^{\theta_i} E^{\theta_i} \tag{10}$$

$$F^\theta_{\max} = \max\left\{ F^{\theta_i}_{\max} \right\} \tag{11}$$

where θ_i is the angle of the applied load (0°, 10°, 20°, and 30°); w^{θ_i} is the weighting factors for different loading angles, which range from 0 to 1. The weighting factors for the four loading angles are given the identical value of 0.25.
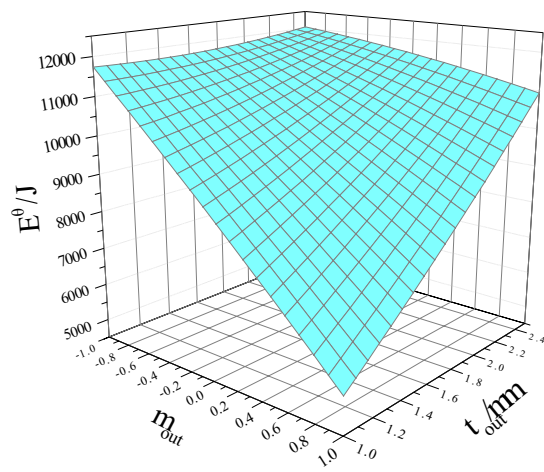
6.3.2 Response surface model

The sample points describing the computed crashworthiness performance of the FGT double tube, as indicated in Table 9, are used to establish response surface models in the overall mass (M), the maximum initial peak force ($F^\theta_{\max}$), and the comprehensive energy absorption capacity (E^θ). These are illustrated in Figs. 19 and 20 for the FGT B9 double tube, respectively, concerning the design variables (m_{out}, t_{out}, m_{in}, and t_{in}).

Figures 19 and 20 demonstrate that the maximum initial peak force and comprehensive energy absorption capacity

Table 9 Sampled points and corresponding crashworthiness performance of double tubes under different loading angles

No	m_{out}	t_{out}/mm	m_{in}	t_{in}/mm	M/g	E^θ/J	$F^\theta_{\max}$/kN
1	0.083	2.062	0.500	2.500	914.29	11,498.25	160.95
2	− 1.000	1.938	− 0.250	1.438	966.65	12,310.00	131.61
3	− 0.833	1.125	− 0.167	1.688	942.49	11,465.50	103.92
4	0.667	1.812	− 0.917	1.500	855.70	9580.75	118.58
5	0.250	1.000	0.667	1.562	634.05	6463.75	83.69
6	− 0.333	1.500	− 0.833	1.125	941.98	11,400.50	102.58
7	− 0.667	1.438	0.750	1.250	784.50	8846.00	100.08
8	0.333	1.875	1.000	1.625	725.53	8258.50	116.83
9	0.833	2.312	− 0.083	1.188	826.97	10,094.25	122.83
10	− 0.417	1.375	0.917	2.125	862.59	10,193.50	121.79
11	0	1.688	0	1.750	846.54	10,294.75	119.07
12	0.917	1.250	− 0.583	2.062	735.43	7868.75	114.64
13	0.750	1.312	0.583	2.25	697.65	7817.75	114.38
14	− 0.917	1.750	0.083	2.375	994.33	12,038.25	147.51
15	− 0.750	2.188	0.833	1.875	896.02	10,848.25	147.67
16	− 0.500	1.625	− 1.000	2.000	995.09	11,343.50	138.2
17	0.583	1.562	0.333	1.000	632.97	6369.75	87.02
18	− 0.583	2.438	− 0.500	2.188	1022.07	12,411.75	171.77
19	− 0.250	2.250	0.417	1.062	800.02	9148.50	119.64
20	0.167	2.500	0.250	1.812	896.74	11,624.00	151.54
21	− 0.083	1.188	− 0.333	2.438	884.87	10,679.50	123.88
22	0.500	1.062	− 0.417	1.312	709.11	7745.25	83.94
23	0.417	2.125	− 0.667	2.312	931.38	10,801.00	160.49
24	− 0.167	2.375	− 0.750	1.375	986.28	12,300.25	138.86
25	1.000	2.000	0.167	1.938	795.79	9715.25	139.55

(a) m_{out}-t_{out}-E^{θ}
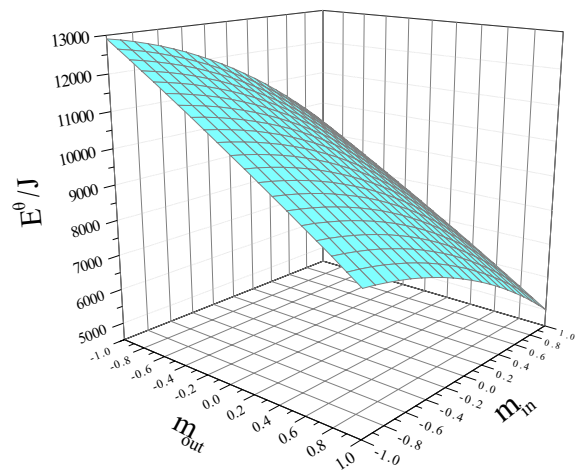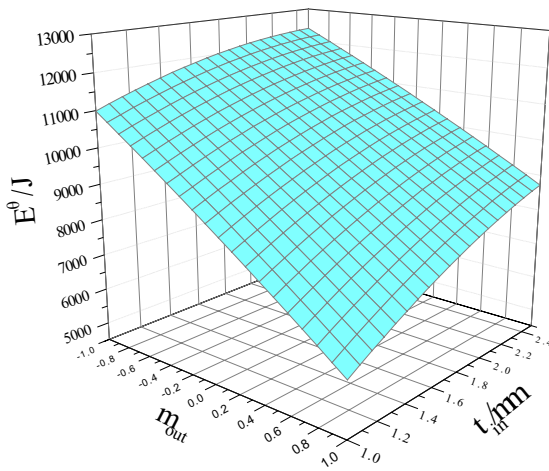
(b) m_{out}-m_{in}-E^{θ}
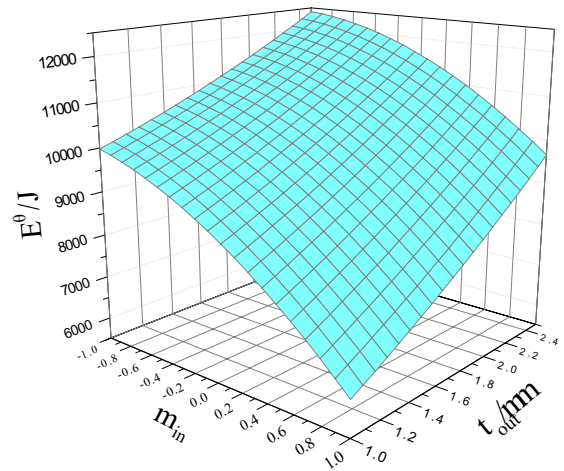
(c) m_{out}-t_{in}-E^{θ}
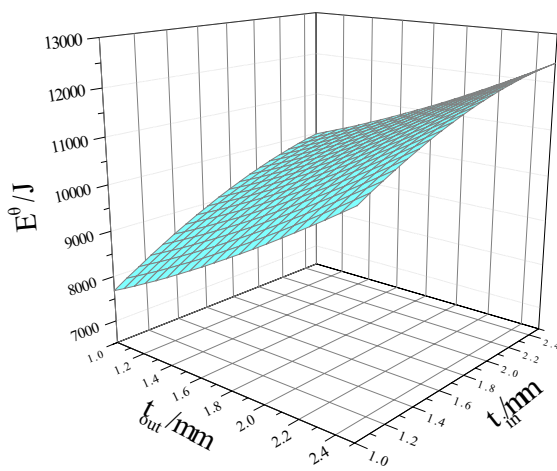
(d) m_{in}-t_{out}-E^{θ}
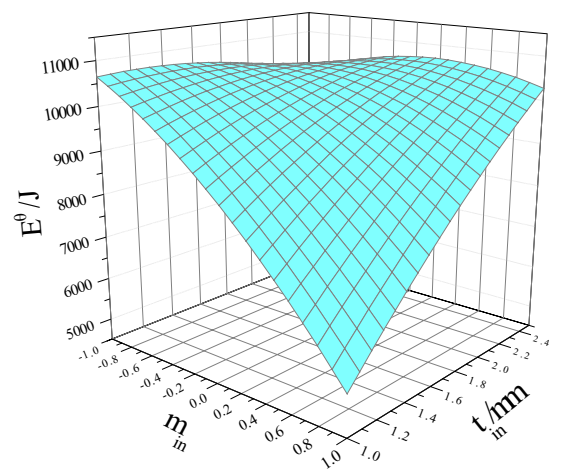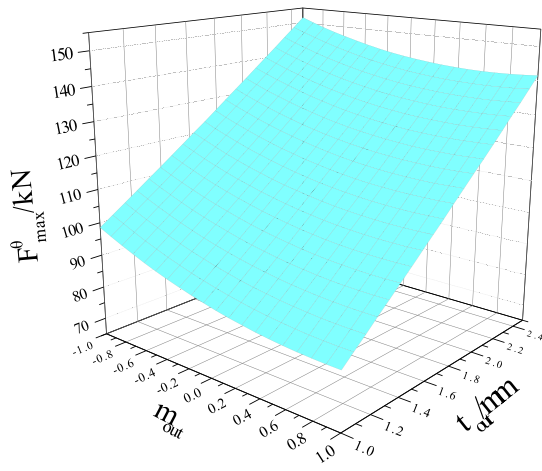
(e) t_{out}-t_{in}-E^{θ}
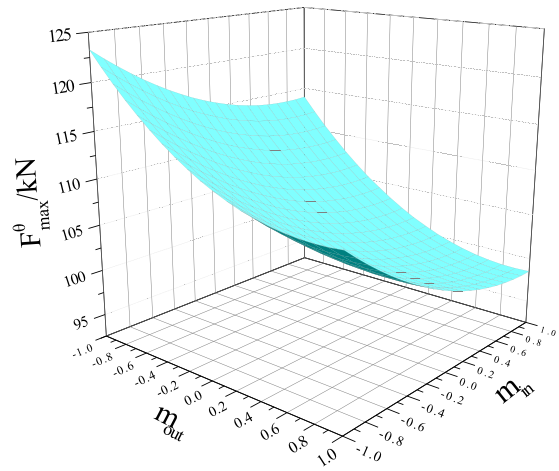
(f) m_{in}-t_{in}-E^{θ}

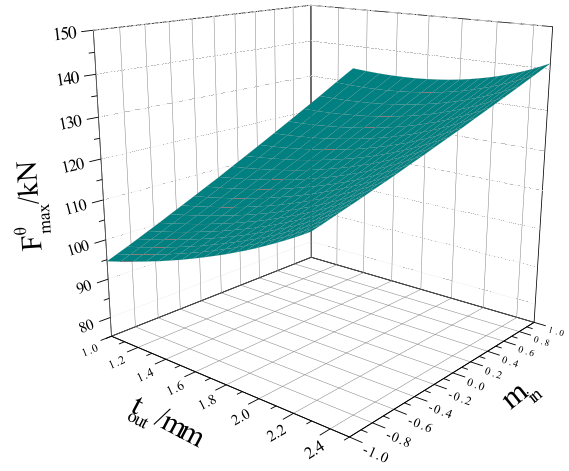**Fig. 19** Spatial response surface of comprehensive energy absorption capacity for FGT double tube
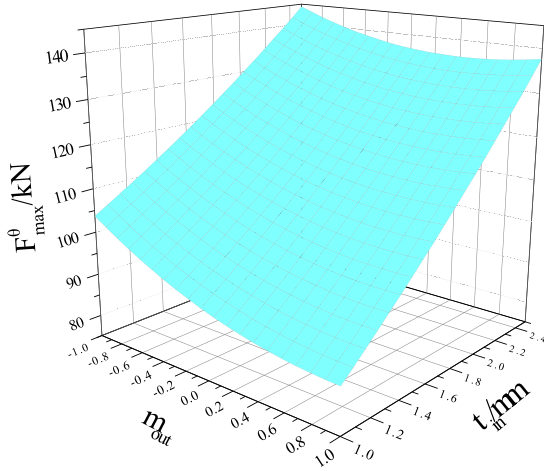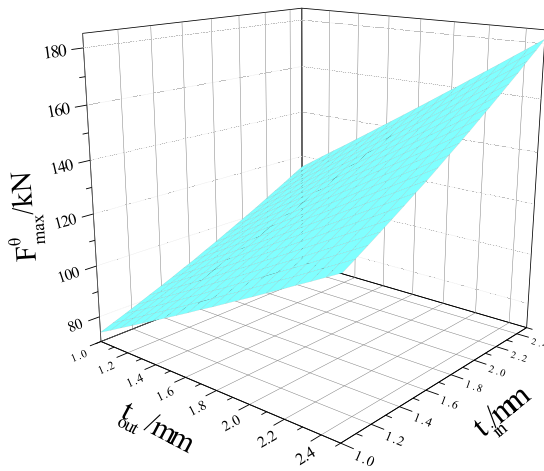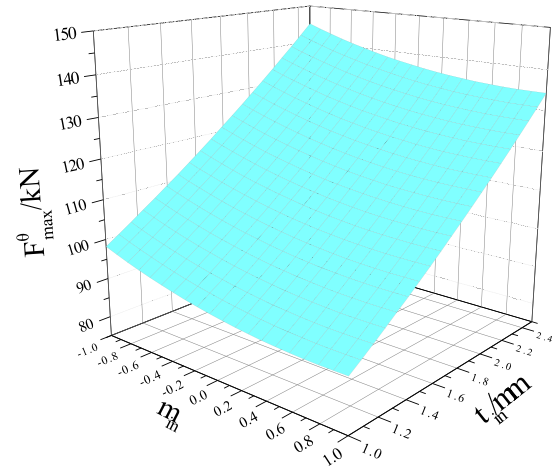
Fig. 20 Spatial response surface of maximum initial peak force for FGT double tube

of the FGT double tube can be enhanced by reducing the gradient values (m_{in} and m_{out}) of the inner and outer tubes and increasing their minimum thicknesses (t_{in} and t_{out}). The optimal structural parameters cannot be immediately identified by these response graphics because the initial peak force and energy absorption capacity are a pair of contradicting indices of each other. The FGT double tube, as an energy-absorbing device, should, nevertheless, have a higher energy absorption capacity and a lower initial peak force. Therefore, the multiobjective optimization technique is applied to get these ideal structural parameters.

6.3.3 Model error analysis

The validity of the response surface model is evaluated in terms of the correlation coefficients (R^2), the root mean square error (P_{RMSE}), and the maximum relative error (Q_{MARE}) (Shen et al. 2017):

$$R^2 = 1 - \frac{\sum_{i=1}^{L}(y_i - \hat{y}_i)^2}{\sum_{i=1}^{L}(y_i - \bar{y}_i)^2} \tag{12}$$

$$P_{RMSE} = \sqrt{\frac{\sum_{i=1}^{L}\left(y_i - \bar{y}_i\right)^2}{\sum_{i=1}^{L}\bar{y}_i}} \tag{13}$$

$$Q_{MARE} = \max_{i=1,2,\ldots,L}\left(\frac{|\hat{y}_i - y_i|}{|y_i|}\right), \tag{14}$$

where L represents the number of newly generated validation points, y_i and $\hat{y}_i$ represent response values determined via the simulation calculation and the approximate models, respectively, on the validation points, and $\bar{y}_i$ represents the mean value of y_i. A higher value of R^2 together with a low value of P_{RMSE} suggests a good fit of the model with higher overall prediction accuracy, while a lower value of Q_{MARE} is desirable for higher local accuracy in the vicinity of a newly generated point.

Results obtained from the simulation computation are used to evaluate the validity and prediction accuracy of the approximation models by generating ten extra sample points in the design space. Table 10 summarizes the measures of the models for the total mass (M), the maximum

initial peak force (F^θ_{max}), and the comprehensive energy absorption capacity (E^θ) for the FGT double tube. It can be seen from the table that the correlation coefficients (R^2) of all approximate models are very close to 1, as well as the root mean square error (P_{RMSE}) and the maximum relative error (Q_{MARE}) are both very small, which indicates that the response surface models can provide accurate predictions of the responses in the considered design space and can be applied to the subsequent crashworthiness optimization.

6.3.4 Multiobjective optimization

Using the gradient index and minimum thickness of the inner and outer tubes as design variables, the total mass and comprehensive energy absorption capacity as the optimization objective, and the maximum initial peak force as the constraint, the crashworthiness optimization problem for the FGT double tube is defined as follows:

$$\begin{cases} \min\left\{-E^\theta\left(m_{out}, t_{out}, m_{in}, t_{in}\right), M\left(m_{out}, t_{out}, m_{in}, t_{in}\right)\right\} \\ F^\theta_{max}\left(m_{out}, t_{out}, m_{in}, t_{in}\right) \leq F \\ m^{min} \leq m_{out}, m_{in} \leq m^{max}, t^{min} \leq t_{out}, t_{in} \leq t^{max} \end{cases} \tag{15}$$

where $M\left(m_{out}, t_{out}, m_{in}, t_{in}\right)$, $E\left(m_{out}, t_{out}, m_{in}, t_{in}\right)$, and $F^\theta_{max}\left(m_{out}, t_{out}, m_{in}, t_{in}\right)$ are the response surface models of the overall mass, the comprehensive energy absorption capacity, and the maximum initial peak force of the double tube, respectively; m^{min} and m^{max} are the minimum and maximum values of the gradient index for the inner and outer tubes, respectively, and its range falls between [-1,1]; t^{min} and t^{max} are the minimum and maximum values of the minimum thickness for the inner and outer tubes, respectively, and its range falls between [1 mm, 2.5 mm]. When carrying out the crashworthiness optimization, $F^\theta_{max}\left(m_{out}, t_{out}, m_{in}, t_{in}\right)$ is specified as a constraint, and its value is constrained to be less than 130 kN.

The optimization problem in Eq. (15) is solved using the non-dominated sorting genetic algorithm (NSGA-II). NSGA-II is an improved version of the genetic algorithm, and it offers enhanced computational efficiency and convergence. The relevant NSGA-II parameters are summarized in Table 11.

Table 10 Assessment of the response surface models for the FGT double tube

Model	R^2	P_{RMSE}	Q_{MARE}
M	0.9973	0.0169	0.0285
E^θ	0.9723	0.0575	0.1029
F^θ_{max}	0.9849	0.0342	0.0649

Table 11 Parameters for NSGA-II

Parameters	Value
Population size	20.0
Number of generations	100.0
Crossover probability	0.9
Crossover distribution index	10.0
Mutation distribution index	20.0

Table 12 Comprehensive energy absorption capacity, maximum initial peak force, and structural parameters of the optimal FGT double tube

m_{out}	t_{out}/mm	m_{in}	T_{in}/mm	M/g	E^{θ}/J	F^{θ}_{max}/kN
0.509	2.317	0.579	1	718.28	8549	114.43

Table 13 Comparison of comprehensive crush performance between uniform thickness and FGT double tube

Index	Uniform thickness	Optimal FGT	Improvement/%
M/g	718.08	718.28	–
E^{θ}/J	7620	8549	12.19
F^{θ}_{max}/kN	130.39	114.43	– 12.24

Figure 21 depicts the optimal Pareto fronts of the FGT double tube under multiple impact angles. The overall mass (*M*) of the FGT double tube is restricted to 718 g, which is the overall mass of the B9 double tube with uniform thickness. Table 12 displays the comprehensive energy absorption capacity, the maximum initial peak force, and the structural parameters of the optimal FGT double tube for a specified overall mass.

After determining the optimal FGT double tube, the comprehensive crushing performances of the uniform thickness and FGT double tubes are compared and analyzed. As shown in Table 13, the comprehensive energy absorption capacity of the double tube may be increased by 12.19%, and the maximum initial peak force may be decreased by 12.24% by adopting a gradient thickness instead of a uniform thickness for a given overall mass, so as to improve the energy absorption characteristics.
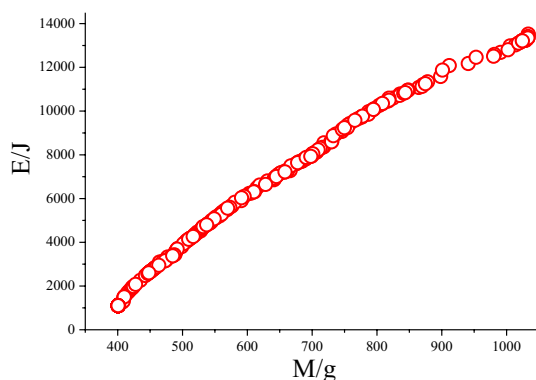
Fig. 21 Pareto fronts of FGT double tube under multiple impact angles

7 Conclusions

(1) The energy absorption characteristics of polygonal single and double tubes under different loading angles are studied. Under axial and small-angle oblique loadings, the double tube has a higher specific energy absorption and energy absorption capacity than the single tube. The energy absorbed by the double tube is more than the sum of the energy absorbed by the inner and outer tubes when loaded individually due to the interaction between them during the crushing deformation process. The energy absorption properties of the double tube are more sensitive to the loading angle, and it is more likely to undergo global bending deformation under oblique loading at large angles, which causes a significant reduction in its specific energy absorption that is even smaller than that of the single tube.

(2) The B9 double tube is determined to have the best comprehensive energy absorption characteristics after being subjected to the comprehensive performance evaluation procedure, considering four loading angles and four performance indices.

(3) The double tube is constructed with a gradient thickness along its axial direction instead of a uniform thickness to optimize its energy absorption capabilities under large-angle oblique loading and raise its critical angle at which global bending deformation occurs. The gradient index and the minimum thickness of the inner and outer tubes have a significant influence on the energy absorption characteristics of the FGT double tube. The energy absorption characteristics of the FGT double tube are enhanced further by the optimization design technique. The comprehensive energy absorption capacity of the optimal FGT double tube is 12.19% higher, and the maximum initial peak force is 12.24% lower than those of the uniform thickness double tube for a given overall mass when the maximum initial peak force is constrained to 130 kN.

References

Chen Y, Bai Z, Zhang L, Wang Y, Sun G, Cao L (2017) Crashworthiness analysis of octagonal multi-cell tube with functionally graded thickness under multiple loading angles. Thin-Walled Struct 110:133–139

Deng X, Liu W (2019) Experimental and numerical investigation of a novel sandwich sinusoidal lateral corrugated tubular structure under axial compression. Int J Mech Sci 151:274–287

Djamaluddin F (2023) Crash behavior and optimization of double tubes with different cross section. Int J Crashworthiness 28:280–287

Djamaluddin F, Abdullah S, Ariffin AK, Nopiah ZM (2015) Optimization of foam-filled double circular tubes under axial and oblique impact loading conditions. Thin-Walled Struct 87:1–11

Du Y, Cao H, Liu F, Yan P, Li C (2011) Evaluation of machine tool remanufacturing scheme based on entropy weight and AHP. Comput Integr Manuf Syst 17(1):84–88

Fang J, Gao Y, Sun G, Qiu N, Li Q (2015) On design of multi-cell tubes under axial and oblique impact loads. Thin-Walled Struct 95:115–126

Fang J, Gao Y, An X, Sun G, Chen J, Li Q (2016) Design of transversely-graded foam and wall thickness structures for crashworthiness criteria. Compos B Eng 92:338–349

Gan N, Yao S, Dong H, Xiong Y, Liu D, Pu D (2018) Energy absorption characteristics of multi-frusta configurations under axial impact loading. Thin-Walled Struct 122:147–157

Gao Q, Wang L, Wang Y, Wang C (2016a) Crushing analysis and multiobjective crashworthiness optimization of foam-filled ellipse tubes under oblique impact loading. Thin-Walled Struct 100:105–112

Gao Q, Wang L, Wang Y, Guo F, Zhang Z (2016b) Optimization of foam-filled double ellipse tubes under multiple loading cases. Adv Eng Software 99:27–35

Goel MD (2015) Deformation, energy absorption and crushing behavior of single-, double-and multi-wall foam filled square and circular tubes. Thin-Walled Struct 90:1–11

Güden M, Kavi H (2006) Quasi-static axial compression behavior of constraint hexagonal and square-packed empty and aluminum foam-filled aluminum multi-tubes. Thin-Walled Struct 44(7):739–750

Kashani MH, Alavijeh HS, Akbarshahi H, Shakeri M (2013) Bitubular square tubes with different arrangements under quasi-static axial compression loading. Mater Des 51:1095–1103

Kim DK, Lee S (1999) Impact energy absorption of 6061 aluminum extruded tubes with different cross-sectional shapes. Mater Des 20(1):41–49

Li Z, Rakheja S, Shangguan WB (2019) Study on crushing behaviors of foam-filled thin-walled square tubes with different types and number of initiators under multiple angle loads. Thin-Walled Struct 145:106376

Li Z, Rakheja S, Shangguan WB (2020) Crushing behavior and crashworthiness optimization of multi-cell square tubes under multiple loading angles. Proc Inst Mech Eng Part D 234(5):1497–1511

Liu W, Lin Z, He J, Wang N, Deng X (2016) Crushing behavior and multi-objective optimization on the crashworthiness of sandwich structure with star-shaped tube in the center. Thin-Walled Struct 108:205–214

Nia AA, Chahardoli S (2016a) Optimizing the layout of nested three-tube structures in quasi-static axial collapse. Thin-Walled Struct 107:169–181

Nia AA, Chahardoli S (2016b) Mechanical behavior of nested multi-tubular structures under quasi-static axial load. Thin-Walled Struct 106:376–389

Nia AA, Khodabakhsh H (2015) The effect of radial distance of concentric thin-walled tubes on their energy absorption capability under axial dynamic and quasi-static loading. Thin-Walled Struct 93:188–197

Rahi A (2018) Controlling energy absorption capacity of combined bitubular tubes under axial loading. Thin-Walled Struct 123:222–231

Sharifi S, Shakeri M, Ebrahimi Fakhari H, Bodaghi M (2015) Experimental investigation of bitubal circular energy absorbers under quasi-static axial load. Thin-Walled Struct 89:42–53

Shen W, Gu X, Jiang P, Hu J, Lv X, Qian L (2017) Crushing analysis and multiobjective optimization design for rectangular unequal triple-cell tubes subjected to axial loading. Thin-Walled Struct 117:190–198

Sun G, Liu T, Fang J, Steven Grant P, Li Q (2018) Configurational optimization of multi-cell topologies for multiple oblique loads. Struct Multidisc Optim 57(2):469–488

Tran TN, Baroutaji A (2018) Crashworthiness optimal design of multi-cell triangular tubes under axial and oblique impact loading. Eng Failure Anal 93:241–256

Vinayagar K, Kumar AS (2017) Crashworthiness analysis of double section bi-tubular thin-walled structures. Thin-Walled Struct 112:184–193

Xiong F, Wang D, Yin S (2018) Optimization analysis of novel foam-filled elliptical columns under multiple oblique impact loading. Mater Des 156:198–214

Yang S, Qi C (2013) Multiobjective optimization for empty and foam-filled square columns under oblique impact loading. Int J Impact Eng 54:177–191

Ying L, Dai M, Zhang S, Ma H, Hu P (2017) Multiobjective crashworthiness optimization of thin-walled structures with functionally graded strength under oblique impact loading. Thin-Walled Struct 117:165–177

Zhang X, Leng K, Zhang H (2017) Axial crushing of embedded multi-cell tubes. Int J Mech Sci 131:459–470

Zheng G, Wu S, Sun G, Li G, Li Q (2014) Crushing analysis of foam-filled single and bitubal polygonal thin-walled tubes. Int J Mech Sci 87:226–240